Application of a microbial siderophore desferrioxamine B in sunlight/Fe3+/persulfate system: from the radical formation to the degradation of atenolol at neutral pH

Yanlin Wu, Tian Qiu, Yu Wang, Huihui Liu, Weiqiang Sun, Wenbo Dong, Gilles Mailhot

Application of a microbial siderophore Desferrioxamine B in sunlight/Fe^{3+}/persulfate system: from the radical formation to the degradation of Atenolol at neutral pH

Yanlin Wu[a,b,c*], Tian Qiu[a], Yu Wang[a], Huihui Liu[a], Weiqiang Sun[a], Wenbo Dong[a,b], Gilles Mailhot[c]

[a]Shanghai Key Laboratory of Atmospheric Particle Pollution and Prevention, Department of Environmental Science & Engineering, Fudan University, Shanghai 200433, China

[b]Shanghai institute of pollution control and ecological security, Shanghai 200092, China

[c]Université Clermont Auvergne, CNRS, SIGMA Clermont, Institut de Chimie de Clermont-Ferrand, F-63000 Clermont-Ferrand, France

Abstract

The present work reported a modified persulfate activation process with a microbial siderophore named Desferrioxamine B (DFOB). DFOB was a natural complexing agent and could complex with Fe^{3+} strongly. The photochemical reactivity of Fe(III)-DFOB was studied. Fe^{2+} and $HO^{\bullet}$ were produced from Fe(III)-DFOB photolysis. Furthermore, the degradation of Atenolol (ATL) was followed in light/persulfate (PS)/Fe(III)-DFOB system. The main oxidative radicals were $SO_4^{\bullet-}$ in this system. The results of pH effect showed that there was no obviously fluctuation on ATL degradation efficiency with the pH increased from 2.5 to 8.4. Moreover, $k_{SO4\bullet-,DFOB}$ was determined by laser flash photolysis (LFP) experiments. DFOB had positive effect on Fe^{2+} formation but negative effect on ATL degradation due to the high react rate constant between DFOB and $SO_4^{\bullet-}$. The effects of chloride and carbonate ion were also investigated. The results in this study proposed the reaction mechanism of the modified persulfate

* Corresponding author. Tel.: +86 21-31242030.
E-mail addresses: wuyanlin@fudan.edu.cn (Y. Wu).

activation process and it could be applied in neutral and weak-alkaline pH range.

Keywords

siderophore, iron complex, neutral pH, sulfate radical, AOPs

Introduction

Fe is an integral element for many living organisms including human, animal, plants and microorganism. However, the most common forms of Fe are iron oxide and iron hydroxide which are difficult to be utilized by organisms (Ratledge and Dover, 2000). The typical concentration of dissolved Fe^{3+} in natural water environment is not higher than 10^{-18} M (Price and Morel, 1998) and it is far below the optimal required concentration for the growth of microbes and plants, 10^{-5}-10^{-7} M and 10^{-4}-10^{-9} M, respectively (Colombo et al. 2014). Thus, the siderophores are produced by cells and they are strong complexing agents to utilize Fe^{3+} in the iron deficiency environment. Siderophores are natural complexing agents and Fe(III)-siderophore complexes are usually formed at neutral pH.

As we well know, ferrous iron is an important activator in traditional Fenton reactions or sulfate radical based advanced oxidation process. The presence of Fe^{2+} related to the photo-reduction of Fe^{3+} from Fe(III) oxides and Fe(III)-complexes (Erel et al. 1993; Johnson et al. 1994). Fe(III)-siderophores, typical iron complexes, could be considered as a potential candidate for Fe(II) formation. Passananti et al. (2016) reported the formation of Fe(II) at pH 6.0 with the irradiation of Fe(III)-Pyoverdin under simulated sunlight. Pyoverdin was a kind of siderophores and produced by the bacterial strain isolated from cloudwater. The formation of Fe^{2+} from the irradiation of Fe(III)-siderophore was confirmed but its application in persulfate activation was not reported as yet.

Desferrioxamine B (DFOB) is a well-known microbial siderophore which is synthesised by fungi and could be found in soils (Farkas et al. 1997; Neubauer et al. 2000). The chemical structure was shown in Fig. S1. It is a hydroxamate-based siderophore which could strongly chelate with Fe^{3+}. The

complexing constant of Fe(III)-DFOB is very high and it was $10^{30.6}$ (Neilands, 1981). Lin et al. (2018) reported the hematite dissolution at different pH in the presence of siderophore DFOB and other three complexing agents (oxalic, citric and malic acid). Total dissolved iron concentration was measured by ICP-OES and the results showed DFOB had positive effect on hematite dissolution at pH 9.0 compared with other organic acids. Borer et al. (2009) studied the dissolution of Lepidocrocite (γ-FeOOH) in the presence of DFOB under different light irradiation. The results showed DFOB could increase the formation of Fe(II) strongly with the decreasing wavelengths below 440 nm at pH 3.0 and Fe(II) was still produced at pH 8.0. It seemed DFOB could not only chelate Fe^{3+} but also release Fe^{2+} with a wide pH range. The characteristics and photoreactivity of Fe(III)-DFOB were investigated in this study. The application of DFOB in persulfate activation for the degradation of pharmaceutical contaminants was also studied.

Recently, sulfate radical ($SO_4^{\bullet-}$)-based advanced oxidation technologies have been intensively investigated for the degradation of organic pollutants, including pharmaceuticals and personal care products (PPCPs), endocrine disrupting chemicals (EDCs) and persistent organic pollutants (POPs) (Lian et al. 2017; Fang et al. 2013; Takdastan et al. 2018; Wu et al. 2019a; Wu et al. 2019b). In this study, Fe(III)-DFOB was introduced as the activator of persulfate (PS) under simulated sunlight irradiation. Atenolol (ATL), a wide existence pharmaceutical compound (Ling et al., 2016), was chosen as the model pollutant in this study. The effect of pH on ATL degradation was investigated in light/PS/Fe(III)-DFOB system. The main radicals were identified. The laser flash photolysis experiments were performed to evaluated the second-order reaction rate constant between $SO_4^{\bullet-}$ and DFOB.

Materials and methods

Chemicals

Desferrioxamine B (DFOB) was purchased as the deferoxamine B mesylate ($C_{25}H_{46}N_5O_8NH_2 \cdot CH_4SO_3$, ≥92.5%) from Sigma Aldrich. Ferric perchlorate hydrate ($Fe(ClO_4)_3 \cdot xH_2O$, Fe content 10.0-12.5%) was also obtained from Sigma Aldrich and the exact concentration of Fe(III) was determined by Ferrozine method (described in Analytical Methods section) before using. $Na_2S_2O_8$ (PS), NaOH, NaCl, $HClO_4$, CH_3COOH, Na_2CO_3, CH_3COONa were analytical grade and purchased from Sinopharm Chemical Reagent Co., Ltd. Ferrozine (97%) and terephthalic acid (TA) were purchased from Sigma Aldrich. Atenolol (99%) was purchased from Dr. Ehrenstorfer Gmbh. Methanol (LC/MS grade) was provided by J&K Scientific Co., Ltd. Fe(III)-DFOB solutions were prepared by mixing appropriate volumes of freshly prepared aqueous solutions of $Fe(ClO_4)_3$ and DFOB.

Simulated sunlight assisted activation of persulfate by Fe(III)-DFOB

The mixed solutions (ATL/Fe(III)-DFOB/PS) were irradiated in a 40 mL quartz bottle and the temperature was constant (298 ± 2 K) controlled by water circulation. The reactor was placed at a fixed point with 10 cm from the lamp. Two lamps were set in the middle and equipped with four filters around to remove wavelengths lower than 290 nm. The purpose was to simulate the solar emission spectrum. The emission spectrums and the energy of the lamps were shown in Fig. S2. The figure of the reactor was shown in Fig. S3. The mixed solutions were continuously stirred during the reaction. The reaction samples were taken at the fixed time intervals. The pH value of the solution was adjusted with NaOH or $HClO_4$ which showed negligible effect on the kinetics of pollutant degradation (Lipctnska-Kochany et al., 1995).

Analytical Methods

ATL concentration in the sample was determined by high performance liquid chromatography (HPLC) system (DIONEX U3000, USA) equipped with a photodiode array detector (DAD). The column was a C18 column (CNW, 5 μm×4.6 mm×250 mm). The mobile phase consisted of 0.01 M CH_3COONH_4 and methanol (70:30). The flow rate was 0.8 ml/min and the detection wavelength was 224 nm. The detection limit of ATL concentration was 0.05 mg/L.

The concentration of Fe(II) was determined by Ferrozine method (Stookey, 1970). Fe(II) and Ferrozine could form a stable carmine complex which had the maximum absorption wavelength at 562 nm. The molar absorption coefficient ($\varepsilon_{562\ nm}$) was reported as $2.79\times10^4\ M^{-1}\ cm^{-1}$ (Berlett, et al. 2001). The concentration of Fe(III) was determined as Fe(II) by adding ascorbic acid (0.05 M) to reduce all the Fe(III) to Fe(II). The detection limit of Fe(II) concentration was 0.8 μM.

The steady-state concentration of hydroxyl radical ($HO^{\bullet}$) was measured with a chemical probe (terephthalic acid, TA). TA was used to trap $HO^{\bullet}$ and the products were 2HTA. It was measured by HPLC with fluorescence detection ($\lambda_{excitation}$ = 315 nm, $\lambda_{emission}$ = 425 nm). The formation yield of 2HTA was estimated as 0.28 (Charbouillot et al. 2011) and the $HO^{\bullet}$ steady-state concentration was calculated based on the literature (Li et al. 2016).

Laser flash photolysis experiments

The transient laser flash photolysis (LFP) experiments were performed to determine the second order reaction rate constant for the reactions between DFOB and $SO_4^{\bullet-}$ ($k_{DFOB,\ SO4^{\bullet-}}$). LFP was performed with the excitation wavelength at 266 nm and using a Quanta Ray LAB-150-10 Nd:YAG laser. The transient absorption spectrum of $SO_4^{\bullet-}$ at 0.3 μs was shown in Fig. S4. The detection wavelength of $SO_4^{\bullet-}$ was 450 nm (George and Chovelon, 2002). The samples were mixed with DFOB and PS solution just before the LFP experiment.

Results and Discussion

Characteristics of Fe(III)-DFOB complex

Fe(III)-DFOB complex was formed by Fe(III) and DFOB in specific proportion. The UV-vis spectrums of Fe^{3+}, DFOB and Fe(III)-DFOB were shown in Fig. S5 and the absorption peak of Fe(III)-DFOB was at 430 nm. Job's Method (Job, 1928) was used to determine stoichiometry of the binding event and it was performed to measure the proportion between Fe(III) and DFOB in this study. The concentration of Fe(III) was held constant, but DFOB concentrations were varied. The absorbance of Fe(III)-DFOB at 430 nm with different proportion between Fe(III) and DFOB was shown in Fig. 1. The inflection point on the curve corresponded to the stoichiometry of the two binding partners. It showed that Fe(III)-DFOB complex formed with the mole proportion 1:1.

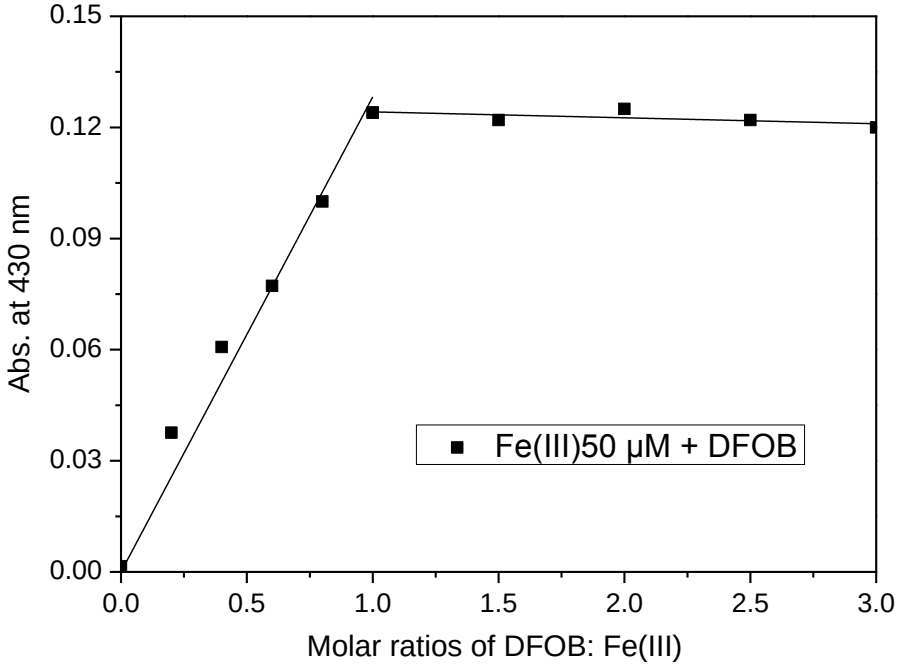

Fig. 1 Effect of molar ratio on the binding of Fe(III) and DFOB (pH=6.5)

DFOB is a hydroxamate-based siderophore with three hydroxamate groups and a terminal primary

amine group. It had four pK_a associated to its structure including pK_{a1} = 8.30, pK_{a2} = 9.00, pK_{a3} = 9.86 and pK_{a4} = 10.84 (Farkas et al. 1999). Thus, DFOB was kept in molecular state in a large pH range. The UV-vis spectra of Fe(III)-DFOB with different pH were shown in Fig. S6. The UV-vis spectra were not affected by different pH showed Fe(III)-DFOB had a very stable form. It might be due to the strong chelating ability of DFOB.

Photochemical behavior of Fe(III)-DFOB complex

The photoactivity of Fe(III)-DFOB was investigated following the degradation of ATL (2.5 mg/L) and formation of Fe(II) in the presence of Fe(III)-DFOB (100 μM) under simulated sunlight irradiation. The results (Fig. S7) showed there was Fe(II) formation at pH 6.5 but almost no degradation of ATL. The conversion rate from Fe(III) to Fe(II) was 10%.

Accompanied by the Fe(II) formation, a series of reactive oxygen species (ROS) such as $HO_2^{\bullet}/O_2^{\bullet-}$, H_2O_2 and $HO^{\bullet}$ would usually be produced according to the photolysis mechanism of many Fe(III)-complexes including Fe(III)-Oxalate (Liu et al. 2010), Fe(III)-Citrate (Feng et al. 2014), Fe(III)-EDDS (Wu et al. 2014) and Fe(III)-Pyoverdin (Passananti et al. 2016). However, ATL was not degraded in light/Fe(III)-DFOB system (Fig. S7). It should be due to the too low concentration of ATL (9.4 μM) compared with 100 μM of DFOB. The ROS was quenched by DFOB. A more sensitive chemical probe (terephthalic acid, TA) was used to trap $HO^{\bullet}$ and the formation of 2HTA was shown in Fig. S8. There was 9.3 μg/L of 2HTA formed after 10 min irradiation of Fe(III)-DFOB. The steady-state concentrations of $HO^{\bullet}$ was calculated as 1.46×10^{-7} M. The formation of $HO^{\bullet}$ could be concluded as shown in Equation (1) to (5). Fe(III)-DFOB with simulated solar light irradiation underwent a ligand-to-metal-charge-transfer (LMCT) leading to Fe(II) formation and organic ligand radicals similar with other Fe(III)-complex (Passananti et al. 2016, Wu et al. 2014, Wang et al. 2012), as shown in Eq. (1). With the reaction with oxygen, $HO_2^{\bullet}/O_2^{\bullet-}$ were formed (Eq. 2-3) and the self-annihilation of them would produce H_2O_2 (Eq. 4) (Bielski et al. 1985). Finally, $HO^{\bullet}$ was produced by the classical Fenton reaction (Eq.5) (Walling and Goosen 1973).

$$\text{Fe(III)} - \text{DFOB} \xrightarrow{h\nu} Fe(II) + DFOB^{\bullet} \qquad (1)$$

$$DFOB^{\bullet} + O_2 \rightarrow DFOB_{ox} + O_2^{\bullet-} \qquad (2)$$

$$O_2^{\bullet -} + H^+ \leftrightarrow HO_2^{\bullet} \qquad pk_a=4.88 \qquad (3)$$

$$O_2^{\bullet -}/HO_2^{\bullet} + HO_2^{\bullet} \rightarrow H_2O_2 + O_2 \qquad (4)$$

$$\text{Fe(II)} + H_2O_2 \rightarrow Fe(III) + OH^- + HO^{\bullet} \qquad (5)$$

Application of DFOB in the activation of PS for ATL degradation at neutral pH

According to the results mentioned above, Fe(II) would be produced from the photolysis of Fe(III)-DFOB. Thus, Fe(III)-DFOB was applied as the source of Fe(II) to activate PS to enhance the ATL degradation. Fig. 2 showed the degradation of ATL in light/Fe(III)-DFOB/PS system. The concentration of Fe(III)-DFOB was set as 15 μM according to the results of pre-experiments (as shown in Table S1). There was almost no degradation of ATL with the directly photolysis. Meanwhile, it was not surprised to see that 12.4% and 45.7% of ATL was degraded after 60 min reaction in PS/light system with 0.1 and 1.0 mM PS. Because PS would be activated by simulated sunlight irradiation directly and $SO_4^{\bullet -}$ would be produced to oxide ATL. The ATL degradation rate was increased to 24% and 60.8% with the addition of Fe(III)-DFOB at pH 6.5. It meant Fe(III)-DFOB could enhance the PS activation even in neutral pH.

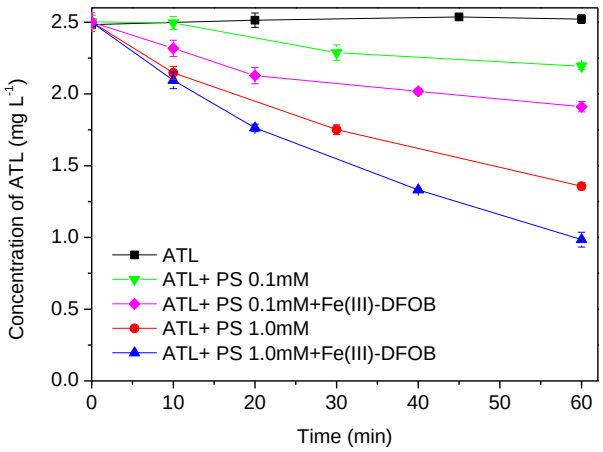

Fig. 2 Degradation of ATL in Fe(III)-DFOB/PS system under simulated sunlight irradiation ([Fe(III)-DFOB]=15 μM, pH=6.5)

pH played an important role in chemical reaction, especially in iron participated oxidation processes because it greatly influenced the speciation of ferric and ferrous iron. The degradation of ATL was followed at different pH in light/PS/Fe(III)-DFOB system. The pseudo-first order reaction rate constants for ATL degradation ($k_{obs,}$ s^{-1}) were calculated according to Eq. (6) and the variety of k_{obs} with different pH was shown in Fig. 3.

$$C_t = C_o e^{-k_{obs}t} \qquad (6)$$

The k_{obs} was 1.269×10^{-4}, 1.385×10^{-4}, 1.349×10^{-4}, 1.317×10^{-4}, 1.103×10^{-4}, 1.1198×10^{-4} s^{-1} when the pH increased from 2.5 to 8.4. It was glad to see there was only slight fluctuation of ATL degradation in such a large pH range. A inhibition was observed at pH 10.0 and the k_{obs} was decreased to 0.876×10^{-4}. However, it was still better than the completely inhibition in UV/PS (Lin et al. 2011) and Fe^{2+}/PS (Xu et al. 2010) processes.

It seems that DFOB could help the Fe(III) dissolve within the pH range of 2.5-8.4 and kept Fe(II) formation. It was a breakthrough compared with the traditional/other Fenton-like processes (Xu et al. 2010; Kattel et al.2017; Costa et al. 2019) which could only be applied in acid pH range. The ATL degradation was almost inhibited at pH 10.0. Because there was no Fe(II) formation due to the alkaline condition. The radicals could only produce from the photolysis of PS. Moreover, many $SO_4^{\bullet-}$ were converted to $HO^{\bullet}$ as expressed in Eq. (7) which had a shorter life. It was also not conducive to ATL degradation.

$$SO_4^{\bullet-} + OH^- \rightarrow SO_4^{2-} + HO^{\bullet} \qquad (7)$$

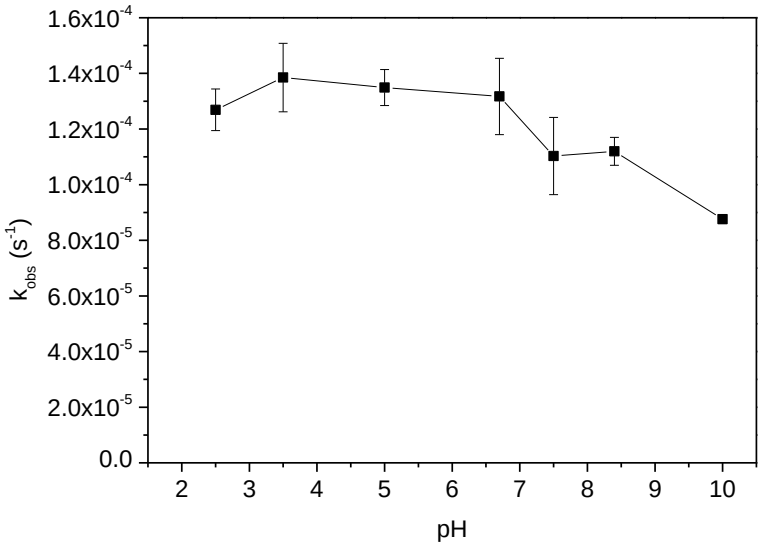

Fig. 3 The variety of ATL degradation efficiency in different pH conditions ([ATL]=2.5 mg/L, [Fe(III)-DFOB]=15 μM, [PS]= 500 μM, pH=6.5)

Identification of radicals

Isopropanol (2-Pr) and ter-butyl alcohol (t-BuOH) with different initial concentrations were used as scavengers in light/PS/Fe(III)-DFOB system. 2-Pr was used as a quencher of both $SO_4^{\bullet-}$ and $HO^{\bullet}$ (Buxton et al.,1988), while t-BuOH was as a scavenger for $HO^{\bullet}$, but not for $SO_4^{\bullet-}$ (Neta et al. 1988). 10 mM t-BuOH was added to quench $HO^{\bullet}$ but not affect the reaction of $SO_4^{\bullet-}$. Different concentrations of 2-Pr were added to completely quench both radicals. The results were shown in Fig. 4. The results demonstrated that both $SO_4^{\bullet-}$ and $HO^{\bullet}$ were responsible for ATL degradation, while $SO_4^{\bullet-}$ was the dominating one. The contribution percentage of each radical was about 85.5% and 14.5%.

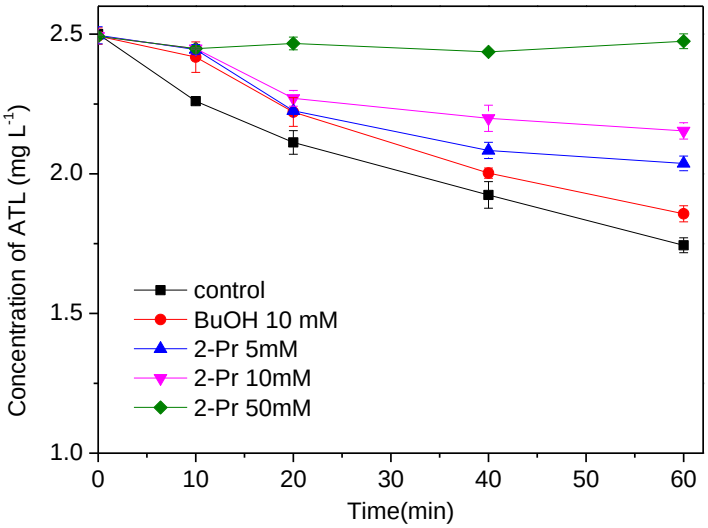

Fig. 4 Effect of different quenchers on ATL degradation ([Fe(III)-DFOB = 15 μM, [PS] = 500 μM, pH = 6.5)

Determination of the second-order rate constant between $SO_4^{\bullet-}$ and DFOB

DFOB as an organic compound would competitively consume radicals. It was very important to estimate the second-order rate constant between $SO_4^{\bullet-}$ and DFOB ($k_{SO4\bullet-,DFOB}$). The transient decay spectra of $SO_4^{\bullet-}$ in the presence of DFOB were obtained via LFP experiments, as shown in Fig. 5(a). The different decay rate constants (k) were obtained when the increasing concentration of DFOB (C_{DFOB}) was added. Fig. 5(b) showed the linear relationship between k and C_{DFOB}. The $k_{SO4\bullet-,DFOB}$ was calculated as $(5.12 \pm 0.33) \times 10^9$ M^{-1} s^{-1}. In our previous study (Wu et al. 2019a), $k_{SO4\bullet-,ATL}$ was estimated as $(8.7 \pm 0.6) \times 10^9$ M^{-1} s^{-1} with the same experimental method. It meant both the chelating agent and target pollutant had very high reactivity with $SO_4^{\bullet-}$. Although DFOB addition could enhance the production of Fe(II), the DFOB concentration should be strictly controlled to prevent it from consuming radicals.

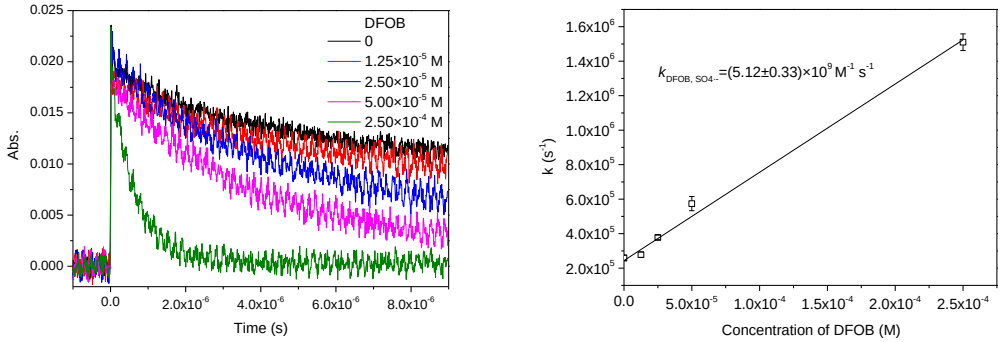

Fig. 5 (a) The transient decay spectra of $SO_4^{\bullet-}$ with different DFOB concentration. (b) Relationship between the pseudo-first order decay of $SO_4^{\bullet-}$ and concentration of DFOB ($[S_2O_8^{2-}]$ = 5.0 mM; pH = 6.50)

Effect of chloride and carbonate ion

Cl^- and HCO_3^-/CO_3^{2-} were the most important anions in water treatment due to their obvious influence on the removal of target pollutants. The degradation of ATL with different concentration of Cl^- (pH=6.5) and HCO_3^- (pH=8) was investigated. The apparent first-order reaction rate constants of ATL degradation with Cl^- and HCO_3^- were calculated respectively, as shown in Table 1. The reaction condition was PS 500 μM and Fe(III)-DFOB 15 μM.

As shown in Table 1, the addition of Cl^- had positive effect on ATL degradation. It was a coincident result with literatures (Wu et al. 2015, Wu et al. 2019a) when Cl^- was added at low concentrations range. Wu et al. (Wu et al. 2019b) used a calculation model to help explain the mechanism. The results of the calculation model showed that low concentrations of Cl^- transformed $SO_4^{\bullet-}$ into $HO^{\bullet}/Cl^{\bullet}$ but the further increased concentration of Cl^- could convert $HO^{\bullet}/Cl^{\bullet}$ into $Cl_2^{\bullet-}$ (with low reactivity) (Eq. 8-11). Moreover, the degradation of ATL in ATL/Cl^-/light system (shown in Fig. S9) showed that $Cl^{\bullet}$ could oxidize ATL directly. So the low concentrations of Cl^- in present study enhanced the degradation of ATL.

234 $SO_4^{\bullet-} + Cl^- \leftrightarrow SO_4^{2-} + Cl^{\bullet}$ (8)

235 $Cl^{\bullet} + OH^- \rightarrow ClOH^{\bullet-}$ (9)

236 $ClOH^{\bullet-} \leftrightarrow OH^{\bullet} + Cl^-$ (10)

237 $Cl^{\bullet} + Cl^- \rightarrow Cl_2^{\bullet-}$ (11)

238 It was normal to see the inhibition of ATL degradation by adding HCO_3^- (Table 1). Because HCO_3^-

239 would quench $SO_4^{\bullet-}$ to produce $CO_3^{\bullet-}$ which was a weak oxidative radical (Wu et al. 2015, Luo et al.

240 2019).

241 $SO_4^{\bullet-} + HCO_3^{2-} \rightarrow SO_4^{2-} + CO_3^{\bullet-} + H^+$ $k_{SO4\bullet-,HCO3-} = 9.1\times10^6\ M^{-1}\ s^{-1}$ (12)

242 Table 1 ATL degradation rate constant with different concentration of Cl^- and HCO_3^-

C_{Cl-} (mg L^{-1})	k_{obs} (s^{-1})	C_{HCO3-} (mg L^{-1})	k_{obs} (s^{-1})
0	1.317×10^{-4}	0	1.317×10^{-4}
10	1.487×10^{-4}	10	9.213×10^{-5}
50	1.658×10^{-4}	50	4.905×10^{-5}
100	2.119×10^{-4}	100	2.719×10^{-5}

243

244

245 ## Conclusions

246 Ferrous iron is the key parameter in PS activation process. A microbial siderophore

247 Desferrioxamine B (DFOB) secreted by fungi was proposed to simultaneously complex with Fe^{3+} and

248 generate Fe^{2+} under simulated sunlight irradiation. The molar proportion between Fe^{3+} and DFOB to

249 form Fe(III)-DFOB complex was 1:1. The photolysis of Fe(III)-DFOB produced Fe(II) and $HO^{\bullet}$. The

250 Fe(II) could be generated even in neutral pH. ATL as the target pollutant could be degraded in

251 light/PS/Fe(III)-DFOB system and the degradation efficiency was kept stable with various pH (2.5-8.4).

252 $SO_4^{\bullet-}$ was the dominating radical which responsible for ATL degradation. $k_{DFOB,\ SO4\bullet-}$ was measured as

253 $(5.12 \pm 0.33) \times 10^9$ $M^{-1}s^{-1}$ by LFP experiments. The high reaction rate constant further proved the both
254 positive and negative sides of DFOB in this reaction. But in any case, the pH range of the modified PS
255 activation process in this study was enlarged to neutral and weak-alkaline pH with a biodegradable
256 compound (DFOB). The chloride ion had slight enhancement of ATL degradation but carbonate ion had
257 inhibition effect. Although the degradation efficiency of ATL was not very high in the experimental
258 condition in this study, the mechanism and the role of DFOB were the focus of this research. The actual
259 work would be guided by the research results.

260 **Acknowledgments**

261 This research was funded by the National Natural Science Foundation of China (NSFC 21607116).

262

263 **References**

264 Berlett BS, Levine RL, Chock PB, Chevion M, Stadtman ER (2001) Antioxidant activity of
265 ferrozine-iron-amino acid complexes. Pro. Natl. Acad. Sci. USA. 98(2), 451-456.
266 Bielski BHJ, Cabelli DE, Arudi RL, Ross AB (1985) Reactivity of HO_2/O_2^- radicals in aqueous
267 solution. J. Phys. Chem. Ref. Data 14, 1041-1100.
268 Borer P, Sulzberger B, Hug SJ, Kraemer SM, Kretzschmar R (2009) Wavelength-dependence of
269 photoreductive dissolution of lepidocrocite (γ-FeOOH) in the absence and presence of the
270 siderophore DFOB. Environ. Sci. Technol. 43(6), 1871-1876.
271 Buxton GV, Greenstock CL, Helman WP, Ross AB (1988) Critical review of rate constants for
272 reactions of hydrated electrons, hydrogen atoms and hydroxyl radicals ($^{\bullet}OH/^{\bullet}O^-$) in Aqueous
273 Solution. J. Phys. Chem. Ref. Data 17, 513-886.
274 Charbouillot T, Brigante M, Mailhot G, Maddigapu P, Minero C, Vione D (2011) Performance and
275 selectivity of the terephthalic acid probe for OH as a function of temperature, pH and composition
276 of atmospherically relevant aqueous media. J. Photochem. Photobiol. A 222 (1), 70-76.
277 Colombo C, Palumbo G, He J, Pinton R, Cesco S (2014) Review on iron availability in soil: interaction
278 of Fe minerals, plants, and microbes. J. Soil. Sediment. 14(3), 538-548.
279 Costa TC, Soares PA, Campos CEM, Souza AAU, Dolic MB, Vilar VJP, Souza SMAGU (2019)
280 Industrial steel waste as an iron source to promote heterogeneous and homogeneous
281 oxidation/reduction reactions. J. Clean. Prod. 211, 804-817.

Erel Y, Pehkonen SO, Hoffmann MR (1993) Redox chemistry of iron in fog and stratus clouds. J. Geophys. Res. 98, 18423-18434.

Fang GD, Dionysiou DD, Zhou DM, Wang Y, Zhu XD, Fan JX, Cang L, Wang YJ (2013) Transformation of polychlorinated biphenyls by persulfate at ambient temperature. Chemosphere. 90(5), 1573-1580.

Farkas E, Csóka H, Micera G, Dessi A (1997) Copper (II), nickel (II), zinc (II), and molybdenum (VI) complexes of desferrioxamine B in aqueous solution. J. inorg. Biochem. 65(4), 281-286.

Farkas E, Enyedy EA, Csóka H (1999) A comparison between the chelating properties of some dihydroxamic acids, desferrioxamine B and acetohydroxamic acid. Polyhedron. 18(18), 2391-3298.

Feng X, Chen Y, Fang Y, Wang X, Wang Z, Tao T, Zuo Y (2014) Photodegradation of parabens by Fe(III)-citrate complexes at circumneutral pH: Matrix effect and reaction mechanism. Sci. Total Environ. 472(15), 130-136.

George C, Chovelon JM (2002) A laser flash photolysis study of the decay of SO_4^- and Cl_2^- radical anions in the presence of Cl^- in aqueous solutions. Chemosphere. 47, 385-393.

Job P (1928) Formation and stability of inorganic complexes in solution. Annali di Chimica Applicata 9(10), 113-203.

Johnson KS, Coale KH, Elrod VA, Tindale NW (1994) Iron photochemistry in seawater from the equatorial Pacific. Mar. Chem. 46, 319-334.

Kattel E, Trapido M, Dulova N (2017) Oxidative degradation of emerging micropollutant acesulfame in aqueous matrices by UVA-induced H_2O_2/Fe^{2+} and $S_2O_8^{2-}/Fe^{2+}$ processes. Chemosphere, 171, 528-536.

Li R, Zhao C, Yao B, Li D, Yan S, O'Shea K, Song W (2016) Photochemical transformation of aminoglycoside antibiotics in simulated natural waters. Environ. Sci. Technol. 50(6), 2921-2930.

Lian L, Yao B, Hou S, Fang J, Yan S, Song W (2017) Kinetic study of hydroxyl and sulfate radical-mediated oxidation of pharmaceuticals in wastewater effluents. Environ. Sci. Technol. 51(5), 2954-2962.

Lin Q, Wang Y, Yang X, Ruan D, Wang S, Wei X, Qiu R (2018) Effect of low-molecular-weight organic acids on hematite dissolution promoted by desferrioxamine B. Environ. Sci. Pollut. R. 25(1), 163-173.

312 Lin YT, Liang C, Chen JH (2011) Feasibility study of ultraviolet activated persulfate oxidation of
313 phenol. Chemosphere. 82(8), 1168-1172.
314 Ling Y, Liao G, Xie Y, Yin J, Huang J, Feng W, Li L (2016) Coupling photocatalysis with ozonation for
315 enhanced degradation of Atenolol by Ag-TiO_2 micro-tube. J. Photochem. Photobio. A 329,
316 280-286.
317 Lipctnska-Kochany E, Sprah G, Harms S (1995) Influence of some groundwater and surface waters
318 constituents on the degradation of 4-chlorophenol by the Fenton reaction. Chemosphere 30(1),
319 9-20.
320 Liu G, Zheng S, Xing X, Li Y, Yin D, Ding Y, Pang W (2010) Fe(III)-oxalate complexes mediated
321 photolysis of aqueous alkylphenol ethoxylates under simulated sunlight conditions. Chemosphere,
322 78(4), 402-408
323 Neilands JB (1981) Microbial iron compounds. Annu. Rev. Biochem. 50(1), 715-731.
324 Neta P, Huie RE, Ross AB (1988) Rate constants for reactions of inorganic radicals in aqueous solution.
325 J. Phys. Chem. Ref. Data 17, 1027-1284.
326 Neubauer U, Nowack B, Furrer G, Schulin R (2000) Heavy metal sorption on clay minerals affected by
327 the siderophore desferrioxamine B. Environ. Sci. Technol. 34(13), 2749-2755.
328 Passananti M, Vinatier V, Delort AM, Mailhot G, Brigante M (2016) Siderophores in cloud waters and
329 potential impact on atmospheric chemistry: Photoreactivity of iron complexes under
330 sun-simulated conditions. Environ. Sci. Technol. 50(17), 9324-9332.
331 Price NM, Morel FMM (1998) Biological cycling of iron in the ocean. Metal ions in biological systems.
332 35, 1-36.
333 Ratledge C, Dover LG (2000) Iron metabolism in pathogenic bacteria. Annu. Rev. Microbiol. 54(1),
334 881-941.
335 Stookey LL (1970). Ferrozine: a new spectrophotometric reagent for iron. Anal. Chem. 42(7), 779-781.
336 Takdastan A, Kakavandi B, Azizi M, Golshan M (2018) Efficient activation of peroxymonosulfate by
337 using ferroferric oxide supported on carbon/UV/US system: a new approach into catalytic
338 degradation of bisphenol A. Chem. Eng. J. 331, 729-743.
339 Walling C, Goosen A (1973) Mechanism of the ferric ion catalyzed decomposition of hydrogen
340 peroxide. Effect of organic substrates. J. Am. Chem. Soc. 95, 2987-2991.
341 Wang Z, Chen C, Ma W, Zhao J (2012) Photochemical coupling of iron redox reactions and

transformation of low-molecular-weight organic matter. J Phys. Chem. Lett. 3(15), 2044-2051.

Wu Y, Bianco A, Brigante M, Dong W, Sainte-Claire P, Hanna K, Mailhot G (2015) Sulfate radical photogeneration using Fe-EDDS: influence of critical parameters and naturally occurring scavengers. Environ. Sci. Technol. 49(24), 14343-14349.

Wu Y, Fang Z, Shi Y, Chen H, Liu Y, Wang Y, Dong W (2019a) Activation of peroxymonosulfate by BiOCl@Fe_3O_4 catalyst for the degradation of atenolol: Kinetics, parameters, products and mechanism. Chemosphere. 216, 248-257.

Wu Y, Passananti M, Brigante M, Dong W, Mailhot G (2014) Fe(III)-EDDS complex in Fenton and photo-Fenton processes: from the radical formation to the degradation of a target compound. Environ. Sci. Pollut. Res. 21, 12154-12162.

Wu Y, Yang Y, Liu Y, Zhang L, Feng L (2019b) Modelling study on the effects of chloride on the degradation of bezafibrate and carbamazepine in sulfate radical-based advanced oxidation processes: Conversion of reactive radicals. Chem. Eng. J. 358, 1332-1341.

Xu XR, Li XZ (2010) Degradation of azo dye Orange G in aqueous solutions by persulfate with ferrous ion. Sep. Purif. Technol. 72(1), 105-111.